

CANCER

Therapeutic inhibition of the SRC-kinase HCK facilitates T cell tumor infiltration and improves response to immunotherapy

Ashleigh R. Poh¹, Christopher G. Love², David Chisanga¹, James H. Steer³, David Baloyan¹, Michaël Chopin⁴, Stephen Nutt⁴, Jai Rautela^{5,6}, Nicholas D. Huntington^{5,6,7}, Nima Etemadi⁴, Megan O'Brien¹, Ryan O'Keefe¹, Lesley G. Ellies³, Christophe Macri⁸, Justine D. Mintern⁸, Lachlan Whitehead⁴, Gangadhara Gangadhara¹, Louis Boon⁹, Ashwini L. Chand¹, Clifford A. Lowell¹⁰, Wei Shi¹, Fiona J. Pixley³, Matthias Ernst^{1*}

Although immunotherapy has revolutionized cancer treatment, many immunogenic tumors remain refractory to treatment. This can be largely attributed to an immunologically “cold” tumor microenvironment characterized by an accumulation of immunosuppressive myeloid cells and exclusion of activated T cells. Here, we demonstrate that genetic ablation or therapeutic inhibition of the myeloid-specific hematopoietic cell kinase (HCK) enables activity of antagonistic anti-programmed cell death protein 1 (anti-PD1), anti-CTLA4, or agonistic anti-CD40 immunotherapies in otherwise refractory tumors and augments response in treatment-susceptible tumors. Mechanistically, HCK ablation reprograms tumor-associated macrophages and dendritic cells toward an inflammatory endotype and enhances CD8⁺ T cell recruitment and activation when combined with immunotherapy in mice. Meanwhile, therapeutic inhibition of HCK in humanized mice engrafted with patient-derived xenografts counteracts tumor immunosuppression, improves T cell recruitment, and impairs tumor growth. Collectively, our results suggest that therapeutic targeting of HCK activity enhances response to immunotherapy by simultaneously stimulating immune cell activation and inhibiting the immunosuppressive tumor microenvironment.

INTRODUCTION

In the past decade, the field of immunotherapy has witnessed remarkable advances for the treatment of patients with cancer. The success of these therapies relies on the capacity of a patient's immune system to kill cancer cells through immune cell-mediated mechanisms. However, durable responses to immunotherapy are limited to select patients, particularly those with immunogenic or “hot” tumors that are densely populated by cytotoxic T cells (1). Meanwhile, patients with refractory tumors show excessive immune suppression and/or insufficient immune activation resulting in an immunologically “cold” tumor microenvironment. The latter is characterized by an abundance of immune suppressive myeloid-derived suppressor cells (MDSCs) and alternatively activated macrophages (AAMs), which promote the exclusion of effector immune cells. Accordingly, therapeutic reprogramming of the immunosuppressive tumor microenvironment can induce robust T cell responses and help overcome the limitations of single-agent immunotherapies (1).

Although aberrant expression of c-SRC and other SRC family kinase members in epithelial cells constitutes oncogenic driver events,

elevated expression and activation of the myeloid-specific SRC family kinase hematopoietic cell kinase (HCK) in the tumor stroma occur in many solid malignancies and correlate with poor patient survival (2). We have previously shown that excessive HCK activity in tumor-associated macrophages (TAMs) enhances the growth of gastric and colon adenomas in Rag1-deficient hosts (3, 4). Here, we reveal that in immunogenic tumors, HCK deficiency unleashes a profound CD8⁺ T cell-dependent antitumor immune response and improves response to immunotherapy. Specifically, genetic ablation of HCK re-educates myeloid cells in the tumor microenvironment toward an inflammatory endotype that enables infiltration of activated effector cells. Meanwhile, therapeutic inhibition of HCK activity in humanized mice reduces the growth of human patient-derived cancer xenografts. Collectively, our results suggest that targeting HCK improves response to immunotherapy by simultaneously remodeling the immunosuppressive tumor microenvironment and by promoting cytotoxic immune cell activation.

RESULTS

Genetic ablation of HCK enhances antitumor responses to anti-PD1 immunotherapy

We have previously shown that genetic ablation of HCK reduces the ability of macrophages to promote the growth of gastric and colon adenomas (3, 4). To determine whether ablation of HCK would improve the response of immunogenic tumors to immunotherapy, we treated wild-type (WT) and HCK knock-out (*Hck*^{KO}) hosts harboring MC38 colon cancer allografts with anti-(α) programmed cell death protein 1 (PD1). We observed reduced tumor growth in *Hck*^{KO} hosts treated with an isotype-matched immunoglobulin G (IgG) control compared to their WT counterparts; however, this was further

Copyright © 2022
The Authors, some
rights reserved;
exclusive licensee
American Association
for the Advancement
of Science. No claim to
original U.S. Government
Works. Distributed
under a Creative
Commons Attribution
NonCommercial
License 4.0 (CC BY-NC).

¹Olivia Newton-John Cancer Research Institute and La Trobe University School of Cancer Medicine, Heidelberg, Victoria 3084, Australia. ²Research Division, Peter MacCallum Cancer Centre, Melbourne, Victoria 3000, Australia. ³School of Biomedical Sciences, University of Western Australia, Crawley, Western Australia 6009, Australia. ⁴Walter and Eliza Hall Institute and Department of Medical Biology, University of Melbourne, Melbourne, Victoria 3052, Australia. ⁵Biomedicine Discovery Institute, Monash University, Clayton, Victoria 3186, Australia. ⁶oNKO-Innate Pty Ltd, Moonee Ponds, Victoria 3039, Australia. ⁷Department of Biochemistry and Molecular Biology, Monash University, Clayton, Victoria 3186, Australia. ⁸Department of Biochemistry and Pharmacology, University of Melbourne and Bio21 Molecular Science and Biotechnology Institute, Melbourne, Victoria 3010, Australia. ⁹JJP Biologics, Warsaw, Poland. ¹⁰University of California, San Francisco, San Francisco, CA 94131, USA.

*Corresponding author. Email: matthias.ernst@onjcri.org.au

augmented in α PD1-treated Hck^{KO} mice compared to all groups (Fig. 1A). These findings were consistent with fewer KI67⁺ proliferating tumor cells in α PD1-treated Hck^{KO} cohorts, as well as a concomitant increase in cleaved Caspase 3⁺ staining indicative of enhanced tumor cell apoptosis (fig. S1A).

To mechanistically link reduced Hck expression in myeloid cells to an improved antitumor immune response, we analyzed the infiltration of myeloid cells between tumors of IgG control isotype- and α PD1-treated WT and Hck^{KO} mice. While HCK deficiency did not affect the overall abundance of TAMs, we observed a marked reduction in CD206⁺ AAMs, CD163⁺ AAMs, and MDSCs in Hck^{KO} hosts irrespective of α PD1 treatment. Tumors recovered from α PD1-treated Hck^{KO} hosts also contained an increased proportion of CD103⁺ conventional dendritic cell 1 (cDC1s) (Fig. 1B). These observations coincided with the similar expression of *Adgre1* (encoding the macrophage marker F4/80) between tumors of IgG isotype- and α PD1-treated WT and Hck^{KO} mice, while transcripts for AAMs (*Mrc1* and *Cd163*) were reduced in Hck^{KO} mice irrespective of α PD1 treatment. We also noted the up-regulated expression of *Xcr1* (indicative of cDC1s) in tumors of α PD1-treated Hck^{KO} hosts compared to all groups (fig. S1B).

To assess how genetic ablation of HCK influenced myeloid cell activation, we isolated TAMs, MDSCs, and DCs from tumors of IgG isotype- and α PD1-treated WT and Hck^{KO} hosts and observed reduced expression of genes associated with immune suppression (i.e., *Il10*, *Il13*, and *Tgfb*) across all myeloid compartments of Hck^{KO} mice irrespective of α PD1 treatment (fig. S1C). Meanwhile, TAMs and DCs purified from α PD1-treated Hck^{KO} mice revealed increased expression of effector genes (i.e., *Il12a*, *Ifny*, *Tnf*, and *Ccr7*) compared to all other cohorts (Fig. 1C). These observations also correlated with the elevated expression of *Cxcl9* and *Cxcl10*, which are two major chemokines involved in the recruitment of cytotoxic natural killer (NK) cells and CD8⁺ T cells (5). Given that interleukin-12 (IL-12) and CXCL9/CXCL10 are primarily produced by myeloid cells (5–8), we next assessed the contribution of these molecules to HCK-dependent suppression of antitumor immunity following administration of neutralizing antibodies directed against either IL-12 or the cognate CXCR3 receptor for the CXCL9/CXCL10 ligands. We observed that blockade of IL-12 or CXCR3 abrogated the beneficial effect of α PD1 therapy in Hck^{KO} hosts, consistent with the requirement for IL-12 and CXCR3 signaling to mediate effective α PD1 antitumor responses in WT mice (Fig. 1D) (5–8). However, tumor growth in α IL-12 or α CXCR3-treated Hck^{KO} hosts was still significantly impaired compared to WT mice treated with these antibodies (Fig. 1D).

To better correlate our in vivo observations with macrophage-specific activities, we compared the ability of IgG- and α PD1-treated bone marrow-derived macrophages (BMDMs) from WT and Hck^{KO} mice to phagocytose MC38 tumor cells in vitro (9, 10). We observed the most profound engulfment of MC38 tumor cells by α PD1-treated Hck^{KO} BMDMs, suggesting that HCK deficiency enhanced the phagocytic profile of macrophages (fig. S1D). Collectively, our results demonstrate that genetic ablation of HCK remodels the immunosuppressive tumor microenvironment by reprogramming myeloid cells to adopt an activated inflammatory endotype.

Next, we assessed the contribution of individual myeloid cell populations to HCK-dependent antitumor immunity. Unexpectedly, α Ly6G-mediated depletion of MDSCs did not confer additional benefit to α PD1 treatment in WT or Hck^{KO} hosts (fig. S1E). To clarify

the contribution of cDC1s and TAMs, we reconstituted lethally irradiated WT hosts with donor bone marrow from either cDC1-deficient [*Itgax*^{Cre}*Irf8*^{fl/fl} (11–13); referred to as cDC1^{KO}] or cDC1-proficient (WT) mice and treated half of each corresponding cohort with a neutralizing antibody against colony-stimulating factor 1 receptor (CSF1R) to also deplete TAMs. Following establishment of subcutaneous MC38 tumors, all hosts were treated with α PD1 in the presence or absence of the HCK-specific small-molecule inhibitor RK20449 (14) (Fig. 1E). Genetic ablation of cDC1s reduced the efficacy of α PD1 therapy in RK20449-treated hosts, consistent with previous studies demonstrating a requirement for cDC1s in restraining MC38 tumor growth (6, 8) (Fig. 1E). Unexpectedly, α CSF1R-mediated depletion of TAMs alone did not affect tumor burden in RK20449-treated hosts. However, simultaneous depletion of both cDC1s and TAMs further abrogated the RK20449-dependent enhanced antitumor response to α PD1 compared to that observed in cDC1-depleted hosts (Fig. 1E).

Genetic ablation of HCK in myeloid cells unleashes CD8⁺ T cell cytotoxicity

We next sought to clarify the contribution of effector/cytotoxic immune cells to the improved antitumor response observed in Hck^{KO} hosts. We observed an increased abundance of CD8⁺ T cells and NK cells in tumors of α PD1-treated Hck^{KO} mice by flow cytometry (Fig. 2A) and up-regulated expression of *CD8a* and *Klrb1c* (encoding the NK cell marker NK1.1) in these samples (fig. S2A). In support of these findings, we noted an increased abundance of CD8⁺ T cells within tumors of α PD1-treated Hck^{KO} hosts compared to all other cohorts (Fig. 2B), despite a similar proportion of KI67⁺ proliferating tumor-associated CD8⁺ T cells across all groups (fig. S2B). CD8⁺ T cells isolated from α PD1-treated Hck^{KO} hosts also contained more granzyme B, interferon- γ (IFN- γ), and tumor necrosis factor- α (TNF α) protein (fig. S2C) and expressed significantly higher levels of *Ifny*, *Prf1*, and *Gzmb* compared to all other cohorts (Fig. 2C). Likewise, we observed more prominent granzyme B and perforin staining in tumor sections of α PD1-treated Hck^{KO} hosts (fig. S2D).

To investigate the contribution of NK cells and CD8⁺ T cells in HCK-mediated tumor suppression, we depleted these cells in WT and Hck^{KO} mice individually before MC38 tumor cell injection and continued until the experimental end point. CD8⁺ T cell depletion abrogated the beneficial effect of α PD1 therapy in both WT and Hck^{KO} hosts (Fig. 2D). In contrast, depletion of NK cells did not affect the antitumor response to α PD1 treatment in WT or Hck^{KO} hosts (Fig. 2E), suggesting that CD8⁺ T cells mediate the enhanced antitumor immunity conferred by Hck^{KO} hosts to α PD1 treatment. We surmise that these effects are largely dependent on IL-12 and CXCR3 signaling by cDC1s and TAMs, since blockade of IL-12 and CXCR3 or depletion of cDC1s and TAMs prominently reduced the enhanced infiltration and cytotoxic activity of CD8⁺ T cells conferred by HCK ablation or inhibition (fig. S2, E to H).

To explore whether systemic HCK activity also promoted cancer progression at more advanced stages of disease, we used an orthotopic breast cancer metastasis model (15). Following resection of the primary EO771.LMB mCherry⁺ tumor from the mammary fat pad of mice, we observed fewer lung metastases in Hck^{KO} hosts compared to WT hosts. This was further augmented in α PD1-treated Hck^{KO} mice (fig. S3A), suggesting that ablation of HCK in hosts significantly reduces lung metastasis and synergizes with α PD1 to sensitize treatment refractory EO771 tumors to immune checkpoint blockade.

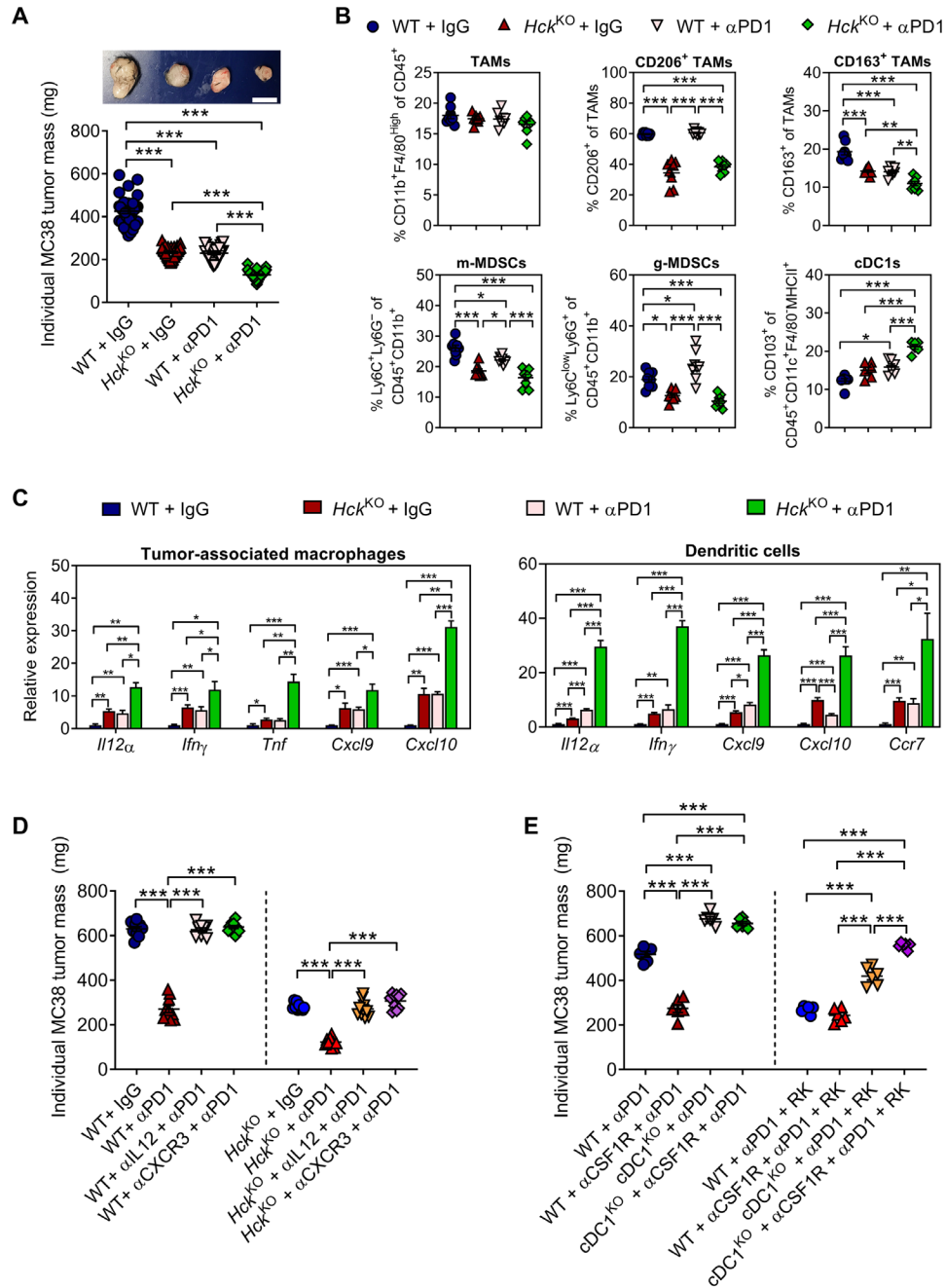


Fig. 1. Genetic ablation of HCK reduces tumor immunosuppression and augments antitumor responses to α PD1 immunotherapy. (A) Mass of individual subcutaneous MC38 tumors from WT and *Hck*^{KO} hosts. Where indicated, mice were treated with α PD1 (200 μ g, once every 3 days) or an isotype-matched IgG control for 10 days. Representative tumors are depicted above the graphs. Scale bar, 1 cm. Each symbol represents an individual mouse. (B) Flow cytometry quantification of the indicated myeloid cell populations from subcutaneous MC38 tumors of WT and *Hck*^{KO} hosts treated as described in (A). Each symbol represents an individual mouse. (C) Quantitative polymerase chain reaction (qPCR) analysis on fluorescence-activated cell sorter (FACS)-purified CD45⁺CD11b⁺F4/80^{High}Ly6C⁻Ly6G⁻ TAMs and CD45⁺CD11c⁺F4/80⁺MHCII⁺ dendritic cells for markers associated with immune cell activation. Cells were isolated from subcutaneous MC38 tumors of WT and *Hck*^{KO} hosts treated as described in (A). *n* = 4 mice per group. (D) Mass of individual subcutaneous MC38 tumors from WT and *Hck*^{KO} hosts. Where indicated, mice were treated with α IL-12, α CXCR3, or an isotype-matched IgG control once every 3 days (total of three treatments) before subcutaneous MC38 tumor cell injection and continued until the experimental end point. Once palpable tumors formed, mice were treated with α PD1 for 10 days. Each symbol represents an individual mouse. (E) Mass of individual subcutaneous MC38 tumors from WT bone marrow chimeras reconstituted with cDC1-deficient (cDC1^{KO}) or cDC1-proficient (WT) bone marrow. To deplete TAMs, half of each cohort were treated with α CSF1R before MC38 tumor cell injection and continued until the experimental end point. Once palpable tumors formed, all hosts were treated with α PD1 in the presence or absence of the small-molecule HCK inhibitor RK20449 for 20 days. Each symbol represents an individual mouse. Data represent mean \pm SEM; **P* < 0.05, ***P* < 0.01, and ****P* < 0.001, with statistical significance determined by one-way ANOVA followed by Tukey's multiple comparison test.

family kinases c-SRC and LYN compared to the clinically approved pan-SRC kinase inhibitor dasatinib (fig. S4A). RK20449 treatment of tumor-bearing WT mice improved the antitumor activity conferred by α PD1 (Fig. 3A). This observation was replicated in

tumor-bearing WT hosts treated with dasatinib (fig. S4B); however, this effect was completely lost when dasatinib was co-administered with α PD1 in tumor-bearing Hck^{KO} hosts (Fig. 3B). From these observations, we surmised that the dasatinib-dependent improvement

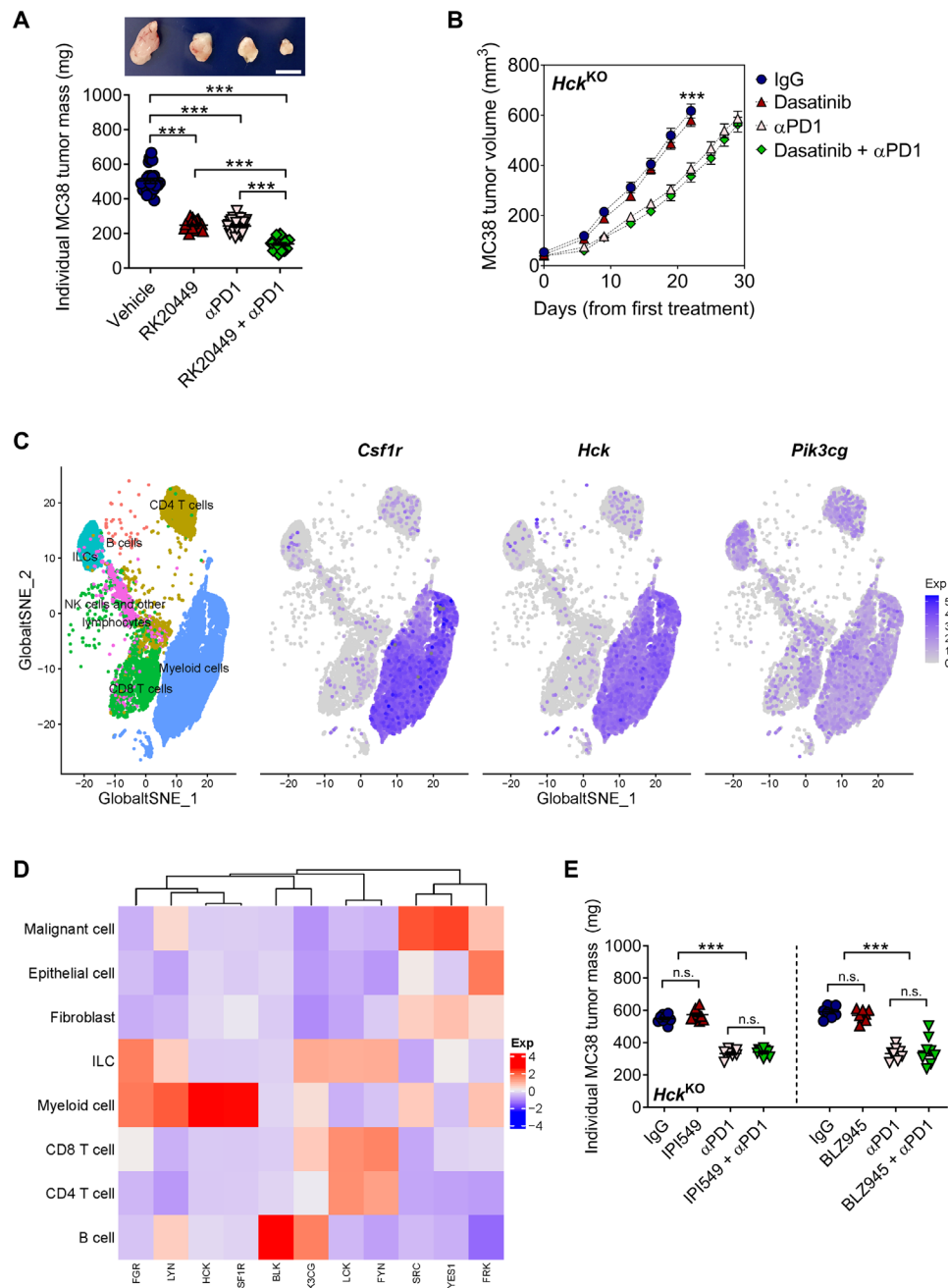


Fig. 3. Therapeutic inhibition of HCK reproduces antitumor immunity observed in Hck^{KO} mice. (A) Mass of individual subcutaneous MC38 tumors from WT hosts treated with RK20449 (30 mg/kg, twice daily) and/or α PD1 (200 μ g, once every 3 days) for a total of 10 days. Vehicle control mice were treated with 12% Captisol and an isotype-matched IgG control. Representative tumors are depicted above graphs. Scale bar, 1 cm. Each symbol represents an individual mouse. (B) Tumor volume of subcutaneous MC38 tumors established in Hck^{KO} hosts treated with dasatinib (30 mg/kg, twice daily) and/or α PD1 (200 μ g, once every 3 days) until the experimental end point when tumors reached $\geq 600 \text{ mm}^3$. $n \geq 9$ mice per group. (C) t-distributed stochastic neighbor embedding (tSNE) plot depicting *Csfr1*, *Hck*, and *Pik3cg* gene expression in subcutaneous MC38 tumors analyzed from Zhang *et al.* (18). (D) Heatmap showing the relative expression of *CSF1R*, *PIK3CG*, *HCK*, and other SFK family members in human colon cancer samples analyzed from Zhang *et al.* (18). (E) Mass of individual subcutaneous MC38 tumors from Hck^{KO} hosts treated with IPI549 (15 mg/kg, once daily) or BLZ945 (200 mg/kg, once daily) in the presence or absence of α PD1 (200 μ g, once every 3 days) for 20 days. Each symbol represents an individual mouse. Data represent mean \pm SEM; *** $P < 0.001$; n.s., not significant, with statistical significance determined by one-way ANOVA followed by Tukey's multiple comparison test.

of α PD1 antitumor immune responses is primarily mediated through inhibition of HCK signaling.

We next extended the validity of HCK as a therapeutic target across a broader range of immune-modulatory agents. Akin to our genetic data, RK20449 treatment of WT hosts improved the therapeutic efficacy of α CD40 in controlling MC38 tumor growth and enabled an α CTLA4 response in WT hosts harboring B16F10 tumors (fig. S4, C and D).

To place HCK with respect to other regulators of myeloid cell activity, we interrogated a single-cell RNA sequencing (scRNA-seq) dataset of MC38 tumors (18) to characterize expression of *Hck* against that of *Pik3cg* [encoding phosphatidylinositol 3-kinase γ (PI3K γ)] (19) and *Csf1r* (20, 21), which are currently pursued as myeloid-specific drug targets. We noted that *Hck* and *Csf1r* were more selectively expressed in myeloid cells than *Pik3cg*, for which we also detected transcripts in B and T lymphocytes and innate lymphoid cells (Fig. 3C). We confirmed these observations in a human colorectal cancer scRNA-seq dataset (18), where we detected *HCK* and *CSF1R* expression exclusively in tumor-associated myeloid cells (Fig. 3D). In contrast, *PIK3CG* was expressed in B and T cells and was less abundant than *HCK* in myeloid cells. Within the family of SRC kinases, we detected strong expression of *SRC*, *YES1*, and *FRK* in cancer epithelial cells, while *FYN* and *LCK* were most prominently expressed in T cells and innate lymphoid cells (Fig. 3D). Together, these findings establish HCK as a myeloid cell-restricted drug target.

Having established a specific expression of *CSF1R* in myeloid cells and broader expression of *PIK3CG* in nonmyeloid cells, we next compared the effect of HCK inhibition against that of *CSF1R* and PI3K γ using the kinase inhibitors BLZ945 and IPI549, respectively, which are both undergoing clinical evaluation for their capacity to boost antitumor immune responses (NCT02829723 and NCT02637531). As single agents, RK20449, IPI549, and BLZ945 inhibited the growth of MC38 tumors in WT mice to a similar extent, and all compounds further augmented the antitumor activity of α PD1 treatment (fig. S4, E and F). Given the reported physical association between *CSF1R* and HCK (22) and between leukocyte integrins and HCK and PI3K γ (19, 23), we next established whether *CSF1R* or PI3K γ inhibition could confer antitumor activity independently of *Hck* gene expression. Unexpectedly, we found that neither BLZ945 nor IPI549 conferred additional tumor-suppressing activity when tested in *Hck*^{KO} hosts harboring MC38 tumors, suggesting linear signaling relationships between HCK and *CSF1R* or PI3K γ , respectively (Fig. 3E). We therefore explored whether HCK activity feeds into the canonical nuclear factor κ B (NF κ B) cascade as proposed for PI3K γ (19) in BMDMs from our HCK allelic series of mice comprising *Hck*^{KO}, WT, and *Hck*^{CA} mice, which harbor an engineered mutation encoding a constitutively active HCK isoform (24). Following stimulation with lipopolysaccharide (LPS) or IL-4, we monitored phosphorylation and degradation of various intermediate NF κ B signaling components. Unlike the reduced NF κ B pathway activation reported by others upon stimulation of *Pik3cg*^{KO} cells (19), we detected similar transient responses in cells across our allelic HCK series, including the rapid and transient reduction of the negative regulator inhibitor of NF κ B α (I κ B α) and the phosphorylation of the p65NF κ B subunit and of the noncanonical I κ B kinase (IKK) kinase TBK1 (TANK Binding Kinase 1) that phosphorylates NF κ B (fig. S4G). Together, our findings suggest that inhibition of HCK and PI3K γ reduces tumor burden only partially through overlapping molecular mechanisms.

Therapeutic inhibition of HCK reduces PDX tumor growth in humanized NSG-SGM3 mice

We next sought to ascertain whether therapeutic inhibition of HCK in human myeloid cells would suppress the growth of human tumors. We therefore adoptively transferred human CD34⁺ hematopoietic stem cells into sublethally irradiated NSG-SGM3 mice and established subcutaneous patient-derived xenografts (PDXs) in the resulting “humanized” NSG-SGM3 recipients. Once palpable tumors formed, we treated mice with RK20449 or vehicle twice daily for 25 days and observed that PDXs grew slower in RK20449-treated hosts (Fig. 4, A and B). This coincided with reduced KI67⁺ proliferating tumor cells in PDXs of RK20449-treated hosts and increased cleaved caspase 3⁺ apoptotic cells and CD3⁺ T cells within tumors (fig. S5A). Furthermore, while the overall proportion of CD68⁺ TAMs remained comparable between PDXs recovered from vehicle- and RK20449-treated hosts, we observed fewer CD163⁺ AAMs in tumors of RK20449-treated mice (fig. S5A).

To exclude the possibility that this effect could be attributed to aberrant HCK expression previously observed in transformed epithelial cells (25), we performed multiplexed immunofluorescence and confirmed that expression of HCK remained restricted to CD45⁺ leukocytes and could not be detected in EPCAM⁺ (Epithelial cell adhesion molecule) tumor cells (fig. S5B). Likewise, Western blot analysis of tumor cell lysates from RK20449-treated hosts confirmed a reduction of activated pHCK but not pSRC and pLYN isoforms (fig. S5C).

Next, we used human-specific probes to interrogate whole PDXs by quantitative polymerase chain reaction (qPCR) analysis for the presence of human immune cells. We noted increased expression of *CD8A*, *NCR2*, and *XCR1* (indicative of CD8⁺ T cells, NK cells and cDC1s) in RK20449-treated mice, while transcripts for human *CD4*, *FOXP3*, and *CD68* (indicative of CD4⁺ T cells, regulatory T cells, and TAMs) remained comparable between tumors recovered from RK20449- and vehicle-treated hosts (Fig. 4C). These observations coincided with increased expression of immune cell activation genes (i.e., *IL12*, *IFNG*, *IL1B*, *TNF*, *CXCL9*, and *CXCL10*) in PDXs of RK20449-treated mice and reduced expression of genes associated with immune suppression (i.e., *CD163*, *MRC1*, *TGFB*, *IL10*, and *CXCL12*) (Fig. 4D).

Last, we determined whether our transcriptional findings in humanized mice extended to patients with cancer. We found that high *HCK* expression was associated with poorer overall, relapse-free, and distant metastasis-free survival in patients with breast cancer using the KMplot tool (26) (fig. S5D), reminiscent of our observations in colon and patients with gastric cancer and the strong correlation between *HCK* gene expression and HCK activity (3, 4). We also analyzed comprehensive datasets from The Cancer Genome Atlas (TCGA) and observed a positive correlation between high *HCK* expression and genes associated with alternative macrophage polarization (i.e., *CD163*, *VSIG4*, and *MS4A7*), T cell exhaustion (i.e., *PDCD1*, *TIGIT*, and *TIM3*), and *CXCL12* and *TGFB1*, which are primarily produced by myeloid cells and limit T cell infiltration into tumors (table S1) (27, 28). To further explore the functional dependency between HCK, immunosuppressive myeloid cell programming, and T cell infiltration, we estimated the relative abundance of these immune cell types in humans using the CIBERSORT tool (29) and confirmed a strong correlation between low *HCK* expression, reduced AAM abundance, and increased CD8⁺ T cells in patients with colon cancer (fig. S5E). Collectively, our findings provide a compelling argument for the translational potential of developing

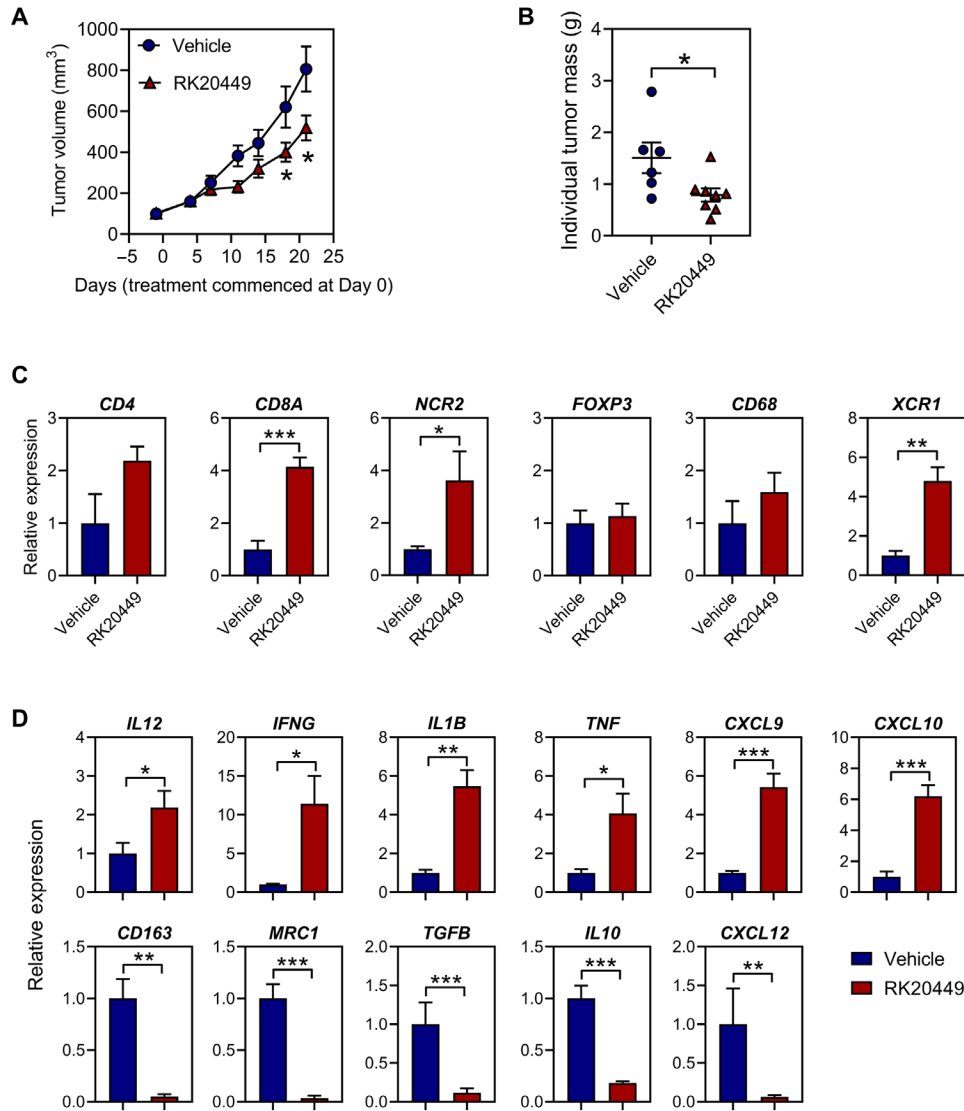


Fig. 4. Therapeutic inhibition of HCK reduces PDX tumor burden in humanized mice. (A and B) Tumor volume and mass of individual subcutaneous PDXs from humanized NSG-SGM3 hosts following treatment with vehicle (12% Captisol) or RK20449 (30 mg/kg, twice daily) for 25 days. Each symbol represents an individual mouse. (C) qPCR analysis on whole PDX tumors from humanized NSG-SGM3 hosts treated as described in (A) for genes associated with human immune cells. $n = 4$ mice per group. (D) qPCR analysis on whole PDX tumors from humanized NSG-SGM3 hosts treated as described in (A) for genes associated with immune cell activation (i.e., *IL12*, *IFNG*, *IL1B*, *TNF*, *CXCL9*, and *CXCL10*) and immune suppression (i.e., *CD163*, *MRC1*, *TGFB*, *IL10*, and *CXCL12*). $n = 4$ mice per group. Data represent mean \pm SEM; * $P < 0.05$, ** $P < 0.01$, and *** $P < 0.001$, with statistical significance determined by an unpaired Student's *t* test.

HCK as a novel myeloid-restricted drug target to boost immune cell activation in patients with cancer.

DISCUSSION

Readily translatable strategies to improve the effectiveness of immunotherapy remain a prime focus in oncology. In this study, we demonstrate that targeting the myeloid-specific kinase HCK overcomes two major barriers that limit the effectiveness of immunotherapy through a suppressive tumor microenvironment and by restricting the recruitment and activation of T cells. Across tumor allograft and PDX models in syngeneic and humanized mice, we show that therapeutic inhibition of HCK reverts the immunosuppressive

tumor microenvironment, enhances T cell infiltration, and promotes the expression of effector genes to collectively reduce tumor growth. Targeting HCK also improves response to immunotherapy.

Among the family of SRC kinases, HCK is the most abundantly expressed member in myeloid cells, which account for 95% of total HCK expression detected in colon cancer PDX models (30). Besides the tumor-promoting function of HCK in TAMs, which we genetically identified by reverting the exaggerated tumor burden of *Hck*^{CA} hosts following ablation of one *Csf1r* allele (3), HCK is also abundantly expressed in DCs, neutrophils, and MDSCs (2, 31). Simultaneous depletion of both cDC1s and TAMs most profoundly abrogated the therapeutic benefit of HCK inhibition, suggesting that HCK expression in these myeloid lineages restricts effective antitumor immune

responses. However, because we could not detect an improved anti-tumor immune response in α PD1-treated hosts following MDSC depletion with α Ly6G, a potential contribution of HCK in MDSCs to cancer control remains unclear. Simultaneous deletion of *Hck* and its closely related family member *Fgr* enhances intracellular signaling and neutrophil chemotaxis in mice (32). Likewise, compound *Hck*^{KO};*Fgr*^{KO} mutant mice show enhanced susceptibility to listeria infection, but neither of these phenotypes were reported in *Hck*^{KO} single-mutant cells and mice, owing to the significant functional overlap between the two kinases (33). While we cannot formally exclude legacy activity of RK20449 against FGR, our previous genetic observations in *Hck*^{KO} hosts argue that the antitumor effects conferred by RK20449 arise primarily from limiting HCK activity (3). We also note that FGR is less abundant than HCK in myeloid cells and down-regulated along the monocyte-macrophage differentiation pathway (34).

Re-education of an immune-suppressive to immune-permissive myeloid tumor microenvironment provides an opportunity to therapeutically exploit the antitumor activity of classically activated macrophages and cDC1s, which play a central role in promoting CD8⁺ T cell recruitment and activation (10, 35). Re-education of myeloid cells is preferred to suppression of myeloid cell maturation in response to CSF1R inhibition, not the least because CSF1R inhibition is associated with elevated liver enzymes and periorbital edema in patients (36, 37). The latter is due to the release of matrix-degrading proteases and proteoglycan deposition (38), reduced endothelial barrier integrity associated with systemic depletion of perivascular macrophages (39), and increased vessel permeability and disordered vascular architecture observed in *Csf1r* ligand-deficient mice (40). Likewise, *Csf1r* deficiency in mice also liberates a compensatory influx of neutrophils and MDSC-like immature monocytes in experimental tumors (36, 37). By contrast, we have identified a functional overlap between HCK and PI3K γ inhibition as a means to re-educate the tumor microenvironment and increase the efficacy of immunotherapy. However, we note that unlike *Hck*^{KO} mice, *Pik3cg*^{KO} mice also display impaired neutrophil chemotaxis, reduced immunoglobulin levels, and increased sensitivity to viral infections amongst other pathologies (41).

Various intracellular molecular mechanisms have been suggested to contribute to the regulation of myeloid endotypes, including canonical NF κ B and STAT (signal transducers and activators of transcription) signaling pathways. For instance, PI3K γ polarizes macrophages by promoting phosphorylation of TBK1, degradation of I κ B α , and engagement of the NF κ B pathway (19, 42). However, we found no difference in NF κ B signaling across our allelic series of HCK mutant macrophages following treatment with LPS or IL-4 to stimulate polarization. While this suggests that HCK does not regulate TAM polarization via the canonical NF κ B signaling cascade as proposed for PI3K γ , previous studies indicate an essential role for HCK in mediating the transcription of inflammatory cytokines and chemokines via activation of TLR4 and NLRP3 (43, 44). Alternative macrophage polarization is also induced by STAT3/STAT6 activity (10), while STAT3 deficiency (or inhibition of STAT3-dependent signaling) is associated with increased expression of type I IFN response genes, including *Cxcl9* and *Cxcl10* (45, 46). Because myeloid cells with excessive HCK activity show increased expression of STAT3- and STAT6-activating cytokines (3, 4), HCK may reinforce AAM polarization and associated cytokine and chemokine expression through autocrine and paracrine STAT3/STAT6 feedback mechanisms.

Collectively, our results provide a strong rationale for HCK to be developed as a therapeutic target to improve antitumor responses to immunotherapy. Its highly restricted expression pattern, the favorable phenotypic consequence of long-term HCK deficiency in mice, and the track record of tyrosine kinases as drug targets provides a novel pathway to improve and expand patient response to immunotherapy.

MATERIALS AND METHODS

Mice

Age- and sex-matched WT, *Hck*^{CA} (24), and *Hck*^{KO} (33) mice were bred and maintained in specific pathogen-free facilities at La Trobe University and the Austin Hospital, Australia. All animal studies were approved and conducted in accordance with the Animal Ethics Committee at the Olivia Newton-John Cancer Research Institute/Austin Hospital.

Subcutaneous tumor models

The mouse MC38 colon cancer (RRID: CVCL_B288) and B16F10 melanoma (RRID: CVCL_0159) cell lines were maintained in Dulbecco's modified Eagle's medium (DMEM)/F12 (Gibco) supplemented with 10% fetal calf serum (FCS) at 37°C with 10% CO₂. Cell lines were tested negative for mycoplasma. Six-week-old C57BL/6 WT or *Hck*^{KO} mice were subcutaneously injected with 2×10^6 MC38 or 2×10^5 B16F10 cells into the right flank. Once palpable tumors formed, mice were randomized into treatment groups.

Where indicated, mice were treated with 12% Captisol [vehicle for RK20449 and dasatinib, intraperitoneally (i.p.)], an isotype-matched IgG control (JPP Biologics, 100 to 200 μ g once every 3 days i.p.), RK20449 (synthesized by Reagency, 30 mg/kg, diluted in 12% Captisol, twice daily i.p.), dasatinib (Selleckchem, #S1021, 30 mg/kg, diluted in 12% Captisol, twice daily i.p.), IPI549 [Selleckchem, #S8330, 15 mg/kg, diluted in 5% dimethyl sulfoxide and 30% PEG300 in ddH₂O, once daily orally (p.o.)], BLZ945 (Selleckchem, #953769-46-5, 200 mg/kg, diluted in 12% Captisol, once daily p.o.), α CD40 (JPP Biologics, clone FGK45, 100 μ g once every 3 days i.p.), α PD1 (JPP Biologics, clone RMP1-14, 200 μ g once every 3 days i.p.), or α CTLA4 (JPP Biologics, clone 4F10, 200 μ g once every 3 days i.p.) for a minimum of 10 days. Immunotherapies produced by JPP Biologics were provided on a collaborative basis. Tumor volume (mm³) was measured using digital calipers using the following formula: (length \times width²)/2. Tumor growth was measured by an independent assessor who was blinded to the experimental conditions.

For antibody-mediated depletion/neutralization experiments, mice were pretreated with α CD8 (JPP Biologics, clone YTS169, 200 μ g), α NK1.1 (JPP Biologics, clone PK136, 200 μ g), α CSF1R (BioCell, #BP0213, clone ASF98, 500 μ g), α Ly6G (BioCell, #BP0075-1, clone 1A8, 200 μ g), α IL-12 (BioCell, #BE0233, clone R2-9A5, 500 μ g), or α CXCR3 (BioCell, #BE0249, clone CXCR3-173, 500 μ g) before subcutaneous tumor injection once every 3 days (total of three treatments) and continued until the experimental end point.

Generation of bone marrow chimeras

Bone marrow was harvested from the femurs and tibias of mice by flushing with sterile phosphate-buffered saline (PBS) as previously described (3, 4). Recipient mice were lethally irradiated with two doses of 5.5-gray γ -irradiation 3 hours apart, before receiving 5×10^6 donor bone marrow cells via tail vein injection. Mice were then maintained

on neomycin-supplemented drinking water for 3 weeks and complete bone marrow reconstitution was assessed 8 weeks later.

EO771 breast cancer metastasis model

EO771.LMB mCherry⁺ breast cancer cells (1×10^5 ; RRID: CVCL_B0A2) (15) were implanted into the fourth inguinal mammary gland of 10-week-old female WT or *Hck*^{KO} hosts as previously described (47). Primary tumors were resected when they reached 800 mm³ in volume to facilitate metastatic spreading of cancer cells to the lung. Following resection of the primary tumor, mice were treated with a matched IgG isotype control or α PD1 (200 μ g, once every 3 days i.p.) for 2 weeks. Genomic DNA was prepared from homogenized lungs, and duplex PCR was performed for mCherry (present in tumor cells) relative to vimentin (housekeeper; present in all cells) using the following sequences: *mCherry*: 5'-GAC-CACCTACAAGGCCAAGAAG-3' (forward) and 5'-AGGTGAT-GTCCAACCTTGATGTTGA-3' (reverse), hydrolysis probe: 5'-FAM-CAGCTGCCCGCGCCTACA-3'-TAMRA; and *Vimentin*: 5'-AGCTGCTAACTACCAGGACACTATTG-3' (forward) and 5'-CGAAGGTGACGAGCCATCTC-3' (reverse), hydrolysis probe: 5'-VIC-CCTTCATGTTTTGGATCTCATCTGCAGG-3'-TAMRA. Metastatic tumor burden was calculated by comparing the quantification cycle (Cq) of mCherry to vimentin using the following equation: $10,000/(2^{\Delta Cq})$, where $\Delta Cq = Cq(\text{mCherry}) - Cq(\text{vimentin})$ as previously described (48).

Humanized mice PDX models

Humanized mice experiments were performed by the Jackson Laboratory (Sacramento, USA) (49). Three-week-old female NSG-SGM3 mice [NOD.Cg-Prkdcscid Il2rgtm1Wjl Tg(CMV-IL3,CSF2, KITLG)1Eav/MloySz]; stock no. 013062] were sublethally irradiated and intravenously reconstituted with human CD34⁺ hematopoietic stem cells (two donors across $n \geq 6$ mice per group). The engraftment levels of mature human CD45⁺ cells were determined 12 weeks following transplantation by flow cytometry quantification of peripheral blood. NSG-SGM3 mice that had >25% human CD45⁺ cells in the peripheral blood were considered engrafted and humanized.

Tumor cells derived from a triple-negative breast cancer PDX were finely minced and subcutaneously injected into the right flank of humanized NSG-SGM3 mice. Once tumors reached approximately 100 mm³ in volume, mice were randomized into treatment groups. Mice were either administered RK20449 (30 mg/kg) or vehicle (12% Captisol) twice daily via intraperitoneal injection for 25 days. Tumor volume (mm³) was measured using digital calipers using the following formula: $(\text{length} \times \text{width}^2)/2$.

Flow cytometry

Tumors were cut into 1-mm pieces and digested in collagenase/dispase (Roche, #11097113001) and deoxyribonuclease I (Roche, #10104159001) in Ca²⁺/Mg²⁺-free Hanks medium (Gibco) plus 10% FCS for 20 min at 37°C under continuous rotation as previously described (3, 4). Samples were vortexed for 30 s to dissociate immune cells, and the cell suspension was filtered and washed in PBS plus 10% FCS. Following incubation with Fc block (Thermo Fisher Scientific, #14-9161-73) on ice for 10 min, cells were incubated with fluorophore-conjugated primary antibodies for 20 min on ice in the dark, washed twice, and resuspended in PBS supplemented with 10% FCS. Intracellular KI67 staining was performed using the eBioscience permeabilization and fixation kit (#88-8824-00) as per

the manufacturer's instructions. Intracellular granzyme B, IFN- γ , and TNF α staining was performed using the BD Biosciences Cytofix/Cytoperm kit (#555028) as previously described (5).

Antibodies for flow cytometry include CD45.2 (clone 30-F11; BioLegend, #103116), F4/80 (clone BM8; BioLegend, #123108 or Thermo Fisher Scientific, #25-4801-82), CD11b (clone M1/70; BD Biosciences, #553311), CD11c (clone 3.9; Thermo Fisher Scientific, #11-0116-42), Ly6G (clone 1A8; BD Biosciences, #560602), Ly6C (clone HK1.4; Thermo Fisher Scientific, #48-5932-82), GR1 (clone RB6-8C5; BioLegend, #108412), CD206 (clone C068C2; BioLegend, #141708), CD163 (clone S15049I; BioLegend, #155306), major histocompatibility complex II (MHC II; clone M5/114.15.2; Thermo Fisher Scientific, #48-5321-82), CD103 (Clone 2E7; Thermo Fisher Scientific, #12-1031-82), NK1.1 (clone PK136; eBioscience, #17-5941-82), T cell receptor β (TCR β ; clone B173150; BioLegend, #109208 or eBioscience, #45-5961-52), CD8a (clone 53-6.7; BD Biosciences, #9150975 or #9186813), CD4 (clone GK1.5; eBioscience, #11-0041-82), KI67 (clone SolA15; eBioscience, #11-5698-82), granzyme B (clone GB11; Thermo Fisher Scientific, #GRB04), IFN- γ (clone 4S.B3; Thermo Fisher Scientific, #14-7319-81), and TNF α (clone MPX-XT22; Thermo Fisher Scientific, #17-7321-82).

Flow cytometry was performed and analyzed on the BD FACS Canto and Aria cell sorter. Analysis was performed using compensated data with FlowJo software (version 10). Background fluorescence was estimated by substituting primary antibodies with their specific isotype controls and/or fluorescent-minus-one controls and by using unstained controls. Dead cells were identified by Sytox Blue (Thermo Fisher Scientific, #S34857) or fixable viability dye (eBioscience, #65-0866-14) staining and excluded from analysis.

RNA extraction and qPCR

RNA extraction on fluorescence-activated cell sorter (FACS)-purified cells was performed using the RN-easy Micro Plus kit (Qiagen, #74034) and complementary DNA (cDNA) was generated with the SuperScript IV First-Strand Synthesis System (Thermo Fisher Scientific, #18091050) according to the manufacturer's instructions. RNA extraction on tumor samples was performed using the RN-easy Mini Plus kit (Qiagen, #74134) and cDNA was generated using the High-Capacity cDNA Reverse Transcription Kit (Thermo Fisher Scientific, #4368814) according to the manufacturer's instructions.

qPCR analysis on each biological sample was performed using technical replicates with Taqman Real-Time PCR Master mix and probes (Thermo Fisher Scientific, #4352042) on the Vii7 Real-Time PCR System for 40 cycles (95°C for 15 s and 60°C for 1 min) and following an initial holding stage (50°C for 2 min and 95°C for 10 min). The cDNA concentration of target genes was normalized by amplification of *18S rRNA* or *Gapdh*/*GAPDH* and fold changes in gene expression were obtained using the $2^{-\Delta\Delta C_T}$ method (50).

Taqman probes for mouse genes were *18s* (Mm04277571_s1), *Gapdh* (Mm99999915_g1), *Cd8a* (Mm01182107_g1), *Cd4* (Mm00442754_m1), *Klrb1c* (Mm00824341_m1), *Adgre* (Mm00802529_m1), *Mrc1* (Mm01329359_m1), *Cd163* (Mm00474091_m1), *Xcr1* (Mm00442206_s1), *Il12a* (Mm00434169_m1), *Ifi1* (Mm01168134_m1), *Tnf* (Mm00443258_m1), *Cxcl9* (Mm00434946_m1), *Cxcl10* (Mm00445235_m1), *Ccr7* (Mm99999130_s1), *Prfl1* (Mm00812512_m1), *Gzmb* (Mm00442837_m1), *Il10* (Mm01288386_m1), *Il13* (Mm00434204_m1), *Tgfb* (Mm01227699_m1), *Arg1* (Mm00475988_m1), and *Ym1* (Mm00657889_mH).

Taqman probes for human genes were *GAPDH* (Hs02786624_g1), *CD68* (Hs04185218_g1), *XCR1* (Hs00245540_s1), *NCR2* (Hs00183113_m1), *CD4* (Hs01058407_m1), *CD8A* (Hs00233520_m1), *FOXP3* (Hs01085834_m1), *TNF* (Hs00174128_m1), *IL12A* (Hs01073447_m1), *CXCL9* (Hs00171065_m1), *CXCL10* (Hs00171042_m1), *IFNG* (Hs00989291_m1), *IL1B* (Hs01555410_m1), *CD163* (Hs00174705_m1), *MRC1* (Hs07288635_g1), *IL10* (Hs00961622_m1), *CXCL12* (Hs00171022_m1), and *TGFB* (Hs00820148_g1).

Immunohistochemistry and immunofluorescence

Paraffin-embedded sections were boiled in citrate buffer for 15 min using a microwave pressure cooker as previously described (3, 4). Slides were incubated in 3% H₂O₂ for 20 min at room temperature to block endogenous peroxidases and then blocked in 10% normal goat serum for 1 hour at room temperature. Primary antibodies were diluted in 10% normal goat serum and incubated at 4°C in a humidified chamber overnight.

For standard immunohistochemical staining, biotinylated secondary antibodies from the Avidin Biotin Complex ABC-kit (Vector Laboratories, #BA-4001 or BA-1000) were used according to the manufacturer's instructions. Antigen visualization was achieved using 3,3-diaminobenzidine (DAKO). Images were collected and analyzed with Aperio ImageScope v1.2.0.780 software. Quantification of positive staining per square micrometer was performed using an automated cell counter script in Fiji (ImageJ).

For immunofluorescence staining, fluorophore-conjugated secondary antibodies (Thermo Fisher Scientific) were incubated for 40 min at room temperature. Akoya Biosciences Spectral DAPI (#FP1490) was used as a nuclei counterstain. Slides were mounted with VECTASHIELD Vibrance anti-fade mounting medium (#H-1700-2). Images were collected using the Vectra 3.0 Automated Quantitative Pathology Imaging System.

Primary antibodies for immunostaining include KI67 (Bethyl Laboratories, #IHC-00375 for mouse or Invitrogen, #PA5-19462 for human samples), cleaved caspase 3 (clone Asp175; Cell Signaling Technology, #9661), CD8a (clone 4SM15; Thermo Fisher Scientific, #14-0808-82), granzyme B (clone D6E9W; Cell Signaling Technology, #44153), perforin (clone E3W4; Cell Signaling Technology, #31647), CD3 (DAKO, #A0452), HCK (clone E117F; Cell Signaling Technology, #14643), EpCAM (clone VU1D9; Cell Signaling Technology, #2929), CD45 (clones 2B11 and PD7/26; Cell Marque, #145M-94), CD68 (clone C68/684; Abcam, #ab201340), and CD163 (clone EPR19518; Abcam, #ab182422).

Isolation and stimulation of BMDMs

Bone marrow was harvested from the femur and tibia of mice by flushing with sterile PBS as previously described (3, 4). Cells were washed twice in PBS and filtered through a 70- μ m sieve. The single-cell suspension was then cultured in macrophage media (DMEM/F12 supplemented with 10% FCS and L929-conditioned media). To fully differentiate BMDMs, cells were cultured for 7 days with fresh media changed every 3 days. Adherent macrophages were detached from plates using a cell scraper, and cell viability was assessed by trypan blue exclusion.

For Western blot analysis, BMDMs were seeded onto six-well plates at a density of 1×10^6 live cells per well in fresh macrophage media. Where indicated, BMDMs were either unstimulated or stimulated the next day with LPS (100 ng/ml; Sigma-Aldrich, #L2630) or murine recombinant IL-4 (20 ng/ml; Peprotech, #214-14). At the

indicated time points, cells were washed with ice-cold PBS, detached from plates using a cell scraper, and processed for Western blot analysis.

BMDM tumor cell phagocytosis assay

BMDMs were isolated and differentiated as outlined above, and BMDM tumor phagocytosis assays were performed as previously described (51). BMDMs (1×10^5) were treated with α PD1 (10 ng/ml) or an isotype-matched IgG (10 ng/ml) control for 24 hours. MC38 cells were labeled with CellTracker Deep Red dye (Invitrogen, #C34565) according to the manufacturer's instructions and cocultured with BMDMs at a 1:1 ratio for 3 hours at 37°C. Cells were washed twice and incubated with Fc block (Thermo Fisher Scientific, #14-9161-73) on ice for 10 min and stained with phycoerythrin-conjugated α CD11b (clone M1/70; BD Biosciences, #553311) and fluorescein isothiocyanate-conjugated α F4/80 (clone BM8; BioLegend, #123108) for 20 min on ice. Cells were washed twice and analyzed by flow cytometry on the BD FACS Canto. Background fluorescence was estimated using fluorescent-minus-one and unstained controls. Dead cells were identified by Sytox Blue (Thermo Fisher Scientific, #S34857) staining and excluded from analysis. Analysis was performed using compensated data with FlowJo software (version 10). Phagocytosis (%) was calculated according to the following formula: (number CD11b⁺F4/80⁺ macrophages positive for CellTracker Deep Red-labeled tumor cells/total number of CD11b⁺F4/80⁺ macrophages) \times 100.

Western blot analysis

Protein lysates were prepared as previously described and resolved on 10% SDS-polyacrylamide gels (3, 4). Following dry transfer, polyvinylidene difluoride membranes were blocked for 1 hour in intercept blocking buffer (LI-COR Biosciences, #927-70001) and incubated overnight in primary antibodies at 4°C. The next day, blots were incubated with fluorescent-conjugated secondary antibodies (LI-COR Biosciences, #926-32221 and #926-32210) for 1 hour. Signals were detected using the Odyssey Infrared Imaging System (LI-COR Biosciences). Actin was used as a loading control.

Primary antibodies for Western blot include pHCK (Abcam, #61055), HCK (Santa Cruz Biotechnology, #N-30), pLYN (Cell Signaling Technology, #2731), LYN (Cell Signaling Technology, #2732), pSRC (Cell Signaling Technology, #2101), SRC (Cell Signaling Technology, #2109), I κ B α (Cell Signaling Technology, #9242), pTBK1 (Cell Signaling Technology, #5483), TBK1 (Cell Signaling Technology, #3504), pp65 (Cell Signaling Technology, #3033), p65 (Cell Signaling Technology, #8242), and Actin (Sigma-Aldrich, #A228 for mouse and Cell Signaling Technology, #3700 for human samples).

Analysis of scRNA-sequencing datasets

scRNA-seq gene expression data of patients with colon cancer previously published (18) and deposited to the National Center for Biotechnology Information's Gene Expression Omnibus database with accession number GSE146771 were downloaded. For this study, we selected the dataset generated using the SMART-seq2 platform, which consisted of already normalized transcript per million (TPM) gene expression values for human colon cancer cells together with their corresponding metadata. In addition, MC38 mouse scRNA-seq normalized gene expression values (TPMs), together with the corresponding metadata, were obtained from the authors (18). The metadata included information on previously identified t-distributed stochastic

neighbor embedding (tSNE) cell clusters and *x-y* coordinates as well as cell-type annotation. The data were first imported into R as a Seurat (52) object after which CD4 T cells were identified based on the cell-type annotation information. tSNE plots were generated using tSNE coordinates for each cell type included in the metadata.

Using the CRC Smart-seq2 human dataset, we compared the expression profile of a set of genes (i.e., *CSF1R*, *PIK3CG*, *HCK*, *FGR*, *SRC*, *LYN*, *FRK*, *YES1*, *FYN*, *LCK*, and *BLK*) in cancer cells, nonimmune cells (epithelium and fibroblasts), innate immune cells (innate lymphoid cells and myeloid cells), and adaptive immune cells (CD8⁺ T cells, CD4⁺ T cells, and B cells). Briefly, the expression values of the gene set in a cell were computed as the geometric mean of all the genes' expression levels and represented as a boxplot to display the variation of cells in each group. A hierarchical clustering of the genes' relative expression across the biological groups was also performed and represented as a heatmap.

Furthermore, using the MC38 mouse dataset, we identified cells that were treated with isotype IgG at days 2 and 10, and generated a tSNE plot comparing the expression levels of *Csf1r*, *Hck*, and *Pik3cg*. To understand the cell types in the lymphocyte population cluster, we performed an unbiased cell annotation analysis on the cells using the Bioconductor package SingleR (53) against the Immunological Genome Project (ImmGen) database available in the celldex Bioconductor package.

TCGA correlation analysis

The TCGA-normalized RNASEQ data were downloaded for colon adenocarcinoma (COAD) using UCSC Xena (54). In total, 283 primary tumor samples were analyzed. Pearson correlations were calculated with the *cor.test* package using R v3.5.1.

CIBERSORT analysis

The relative fraction of immune cell types in high and low *HCK* COAD TCGA samples were estimated using CIBERSORT (29). Immune signatures for CD8⁺ T cells and AAMs were obtained from leukocyte signature LM22 (55). The COAD TCGA gene expression data classified by level of *HCK* expression (<25%, low, *n* = 71 and ≥75%, high, *n* = 71) was deconvoluted using CIBERSORT. High and low relative cell fractions for each immune cell type were tested for statistical significance using a two-tailed Student's *t* test (*P* < 0.05) using R v3.5.1.

Statistics

All experiments were performed at least twice with a minimum of four age- and sex-matched mice per group. The specific *n* (number of animals) used per cohort is indicated in the respective figure legends or shown as individual datapoints. No data were excluded from analysis. Statistical analysis was conducted using GraphPad Prism Software (version 8). For comparison between multiple groups, a one- or two-way analysis of variance (ANOVA) followed by Tukey's multiple comparison test was performed as appropriate. Comparisons between two mean values were performed with a two-tailed Student's *t* test. For survival studies, a Mantel-Cox log-rank test was used to evaluate statistical significance in Kaplan-Meier analysis. A *P* value of less than 0.05 was considered statistically significant.

SUPPLEMENTARY MATERIALS

Supplementary material for this article is available at <https://science.org/doi/10.1126/sciadv.abl7882>

[View/request a protocol for this paper from Bio-protocol.](#)

REFERENCES AND NOTES

1. J. Galon, D. Bruni, Approaches to treat immune hot, altered and cold tumours with combination immunotherapies. *Nat. Rev. Drug Discov.* **18**, 197–218 (2019).
2. A. R. Poh, R. J. J. O'Donoghue, M. Ernst, Hematopoietic cell kinase (HCK) as a therapeutic target in immune and cancer cells. *Oncotarget* **6**, 15752–15771 (2015).
3. A. R. Poh, C. G. Love, F. Masson, A. Preaduet, C. Tsui, L. Whitehead, S. Monard, Y. Khakham, L. Burstroem, G. Lessene, O. Sieber, C. Lowell, T. L. Putoczki, R. J. J. O'Donoghue, M. Ernst, Inhibition of hematopoietic cell kinase activity suppresses myeloid cell-mediated colon cancer progression. *Cancer Cell* **31**, 563–575.e5 (2017).
4. A. R. Poh, A. R. Dwyer, M. F. Eissmann, A. L. Chand, D. Baloyan, L. Boon, M. W. Murrey, L. Whitehead, M. O'Brien, C. A. Lowell, T. L. Putoczki, F. J. Pixley, R. J. J. O'Donoghue, M. Ernst, Inhibition of the SRC kinase HCK impairs STAT3-dependent gastric tumor growth in mice. *Cancer Immunol. Res.* **8**, 428–435 (2020).
5. I. G. House, P. Savas, J. Lai, A. X. Y. Chen, A. J. Oliver, Z. L. Teo, K. L. Todd, M. A. Henderson, L. Giuffrida, E. V. Petley, K. Sek, S. Mardiana, T. N. Gide, C. Quek, R. A. Scolyer, G. V. Long, J. S. Wilmott, S. Loi, P. K. Darcy, P. A. Beavis, Macrophage-derived CXCL9 and CXCL10 are required for antitumor immune responses following immune checkpoint blockade. *Clin. Cancer Res.* **26**, 487–504 (2020).
6. I. C. Arnold, X. Zhang, M. Artola-Boran, A. Fallegger, P. Sander, P. Johansen, A. Müller, BATF3-dependent dendritic cells drive both effector and regulatory T-cell responses in bacterially infected tissues. *PLOS Pathog.* **15**, e1007866 (2019).
7. M. T. Chow, A. J. Ozga, R. L. Servis, D. T. Frederick, J. A. Lo, D. E. Fisher, G. J. Freeman, G. M. Boland, A. D. Luster, Intratumoral activity of the CXCR3 chemokine system is required for the efficacy of anti-PD-1 therapy. *Immunity* **50**, 1498–1512.e5 (2019).
8. C. S. Garriss, S. P. Arlauckas, R. H. Kohler, M. P. Trefny, S. Garren, C. Piot, C. Engblom, C. Pfirschke, M. Siwicz, J. Jungabeesoon, G. J. Freeman, S. E. Warren, S. Ong, E. Browning, C. G. Twitty, R. H. Pierce, M. H. Le, A. P. Algazi, A. I. Daud, S. I. Pai, A. Zippelius, R. Weissleder, M. J. Pittet, Successful anti-PD-1 cancer immunotherapy requires T cell-dendritic cell crosstalk involving the cytokines IFN- γ and IL-12. *Immunity* **49**, 1148–1161.e7 (2018).
9. S. R. Gordon, R. L. Maute, B. W. Dulken, G. Hutter, B. M. George, M. N. McCracken, R. Gupta, J. M. Tsai, R. Sinha, D. Corey, A. M. Ring, A. J. Connolly, I. L. Weissman, PD-1 expression by tumour-associated macrophages inhibits phagocytosis and tumour immunity. *Nature* **545**, 495–499 (2017).
10. A. R. Poh, M. Ernst, Targeting macrophages in cancer: From bench to bedside. *Front. Oncol.* **8**, 49 (2018).
11. M. L. Caton, M. R. Smith-Raska, B. Reizis, Notch-RBP-J signaling controls the homeostasis of CD8⁺ dendritic cells in the spleen. *J. Exp. Med.* **204**, 1653–1664 (2007).
12. J. Feng, H. Wang, D.-M. Shin, M. Masiuk, C.-F. Qi, H. C. Morse III, IFN regulatory factor 8 restricts the size of the marginal zone and follicular B cell pools. *J. Immunol.* **186**, 1458–1466 (2011).
13. M. Chopin, C. Seillet, S. Chevrier, L. Wu, H. Wang, H. C. Morse III, G. T. Belz, S. L. Nutt, Langerhans cells are generated by two distinct PU.1-dependent transcriptional networks. *J. Exp. Med.* **210**, 2967–2980 (2013).
14. Y. Saito, H. Yuki, M. Kuratani, Y. Hashizume, S. Takagi, T. Honma, A. Tanaka, M. Shirouzu, J. Mikuni, N. Handa, I. Ogahara, A. Sone, Y. Najima, Y. Tomabechi, M. Wakiyama, N. Uchida, M. Tomizawa-Murasawa, A. Kaneko, S. Tanaka, N. Suzuki, H. Kajita, Y. Aoki, O. Ohara, L. D. Shultz, T. Fukami, T. Goto, S. Taniguchi, S. Yokoyama, F. Ishikawa, A pyrrolo-pyrimidine derivative targets human primary AML stem cells in vivo. *Sci. Transl. Med.* **5**, 181ra152 (2013).
15. C. N. Johnstone, Y. E. Smith, Y. Cao, A. D. Burrows, R. S. N. Cross, X. Ling, R. P. Redvers, J. P. Doherty, B. L. Eckhardt, A. L. Natoli, C. M. Restall, E. Lucas, H. B. Pearson, S. Deb, K. L. Britt, A. Rizzitelli, J. Li, J. H. Harmey, N. Pouliot, R. L. Anderson, Functional and molecular characterisation of EO771.LMB tumours, a new C57BL/6-mouse-derived model of spontaneously metastatic mammary cancer. *Dis. Model Mech.* **8**, 237–251 (2015).
16. K. R. Wiehagen, N. M. Girgis, D. H. Yamada, A. A. Smith, S. R. Chan, I. S. Grewal, M. Quigley, R. I. Verona, Combination of CD40 agonism and CSF-1R blockade reconditions tumor-associated macrophages and drives potent antitumor immunity. *Cancer Immunol. Res.* **5**, 1109–1121 (2017).
17. A. van Elsas, A. A. Hurwitz, J. P. Allison, Combination immunotherapy of B16 melanoma using anti-cytotoxic T lymphocyte-associated antigen 4 (CTLA-4) and granulocyte/macrophage colony-stimulating factor (GM-CSF)-producing vaccines induces rejection of subcutaneous and metastatic tumors accompanied by autoimmune depigmentation. *J. Exp. Med.* **190**, 355–366 (1999).
18. L. Zhang, Z. Li, K. M. Skrzypczynska, Q. Fang, W. Zhang, S. A. O'Brien, Y. He, L. Wang, Q. Zhang, A. Kim, R. Gao, J. Orf, T. Wang, D. Sawant, J. Kang, D. Bhatt, D. Lu, C.-M. Li, A. S. Rapaport, K. Perez, Y. Ye, S. Wang, X. Hu, X. Ren, W. Ouyang, Z. Shen, J. G. Egen, Z. Zhang, X. Yu, Single-cell analyses inform mechanisms of myeloid-targeted therapies in colon cancer. *Cell* **181**, 442–459.e29 (2020).
19. M. M. Kaneda, K. S. Messer, N. Ralainirina, H. Li, C. J. Leem, S. Gorjestani, G. Woo, A. V. Nguyen, C. C. Figueiredo, P. Foubert, M. C. Schmid, M. Pink, D. G. Winkler, M. Rausch,

- V. J. Palombella, J. Kutok, K. McGovern, K. A. Frazer, X. Wu, M. Karin, R. Sasik, E. E. W. Cohen, J. A. Varner, PI3K γ is a molecular switch that controls immune suppression. *Nature* **539**, 437–442 (2016).
20. E. R. Stanley, V. Chitu, CSF-1 receptor signaling in myeloid cells. *Cold Spring Harb. Perspect. Biol.* **6**, a021857 (2014).
 21. K. Grabert, A. Sehgal, K. M. Irvine, E. Wollscheid-Lengeling, D. D. Ozdemir, J. Stables, G. A. Luke, M. D. Ryan, A. Adamson, N. E. Humphreys, C. J. Sandrock, R. Rojo, V. A. Verkasalo, W. Mueller, P. Hohenstein, A. R. Pettit, C. Pridans, D. A. Hume, A transgenic line that reports CSF1R protein expression provides a definitive marker for the mouse mononuclear phagocyte system. *J. Immunol.* **205**, 3154–3166 (2020).
 22. A. R. Dwyer, K. A. Mouchemore, J. H. Steer, A. J. Sunderland, N. G. Sampaio, E. L. Greenland, D. A. Joyce, F. J. Pixley, Src family kinase expression and subcellular localization in macrophages: Implications for their role in CSF-1-induced macrophage migration. *J. Leukoc. Biol.* **100**, 163–175 (2016).
 23. C. Giagulli, L. Ottoboni, E. Cavegion, B. Rossi, C. Lowell, G. Constantin, C. Laudanna, G. Berton, The SRC family kinases Hck and Fgr are dispensable for inside-out, chemoattractant-induced signaling regulating β 2 integrin affinity and valency in neutrophils, but are required for β 2 integrin-mediated outside-in signaling involved in sustained adhesion. *J. Immunol.* **177**, 604–611 (2006).
 24. M. Ernst, M. Inglese, G. M. Scholz, K. W. Harder, F. J. Clay, S. Bozinovski, P. Waring, R. Darwiche, T. Kay, P. Sly, R. Collins, D. Turner, M. L. Hibbs, G. P. Anderson, A. R. Dunn, Constitutive activation of the SRC family kinase Hck results in spontaneous pulmonary inflammatory and an enhanced innate immune response. *J. Exp. Med.* **196**, 589–604 (2002).
 25. A. Goldman, B. Majumder, A. Dhawan, S. Ravi, D. Goldman, M. Kohandel, P. K. Majumder, S. Sengupta, Temporally sequenced anticancer drugs overcome adaptive resistance by targeting a vulnerable chemotherapy-induced phenotypic transition. *Nat. Commun.* **6**, 6139 (2015).
 26. A. Lanczyk, B. Gyorffy, Web-based survival analysis tool tailored for medical research (KMplot): Development and implementation. *J. Med. Internet Res.* **23**, e27633 (2021).
 27. E. Peranzoni, J. Lemoine, L. Vimeux, V. Feuillet, S. Barrin, C. Kantari-Mimoun, N. Bercovici, M. Guerin, J. Biton, H. Ouakrim, F. Regnier, A. Lupo, M. Alifano, D. Damotte, E. Donnadiou, Macrophages impede CD8 T cells from reaching tumor cells and limit the efficacy of anti-PD-1 treatment. *Proc. Natl. Acad. Sci.* **115**, E4041–E4050 (2018).
 28. D. A. Thomas, J. Massague, TGF- β directly targets cytotoxic T cell functions during tumor evasion of immune surveillance. *Cancer Cell* **8**, 369–380 (2005).
 29. B. Chen, M. S. Khodadoust, C. L. Liu, A. M. Newman, A. A. Alizadeh, Profiling tumor infiltrating immune cells with CIBERSORT. *Methods Mol. Biol.* **1711**, 243–259 (2018).
 30. C. Isella, A. Terrasi, S. E. Bellomo, C. Petti, G. Galatola, A. Muratore, A. Mellano, R. Senetta, A. Cassenti, C. Sonetto, G. Inghirami, L. Trusolino, Z. Fekete, M. De Ridder, P. Cassoni, G. Storme, A. Bertotti, E. Medico, Stromal contribution to the colorectal cancer transcriptome. *Nat. Genet.* **47**, 312–319 (2015).
 31. C.-L. Chu, C. A. Lowell, The Lyn tyrosine kinase differentially regulates dendritic cell generation and maturation. *J. Immunol.* **175**, 2880–2889 (2005).
 32. H. Zhang, F. Meng, C. L. Chu, T. Takai, C. A. Lowell, The Src family kinases Hck and Fgr negatively regulate neutrophil and dendritic cell chemokine signaling via PIR-B. *Immunity* **22**, 235–246 (2005).
 33. C. A. Lowell, P. Soriano, H. E. Varmus, Functional overlap in the src gene family: Inactivation of hck and fgr impairs natural immunity. *Genes Dev.* **8**, 387–398 (1994).
 34. M. W. Murrey, J. H. Steer, E. L. Greenland, J. M. Proudfoot, D. A. Joyce, F. J. Pixley, Adhesion, motility and matrix-degrading gene expression changes in CSF-1-induced mouse macrophage differentiation. *J. Cell Sci.* **133**, jcs232405 (2020).
 35. J. P. Bottcher, C. R. e Sousa, The role of type 1 conventional dendritic cells in cancer immunity. *Trends Cancer* **4**, 784–792 (2018).
 36. T. Beltraminelli, M. De Palma, Biology and therapeutic targeting of tumour-associated macrophages. *J. Pathol.* **250**, 573–592 (2020).
 37. K. P. Papadopoulos, L. Gluck, L. P. Martin, A. J. Olszanski, A. W. Tolcher, G. Ngarmchamnanrith, E. Rasmussen, B. M. Amore, D. Nagorsen, J. S. Hill, J. Stephenson Jr., First-in-human study of AMG 820, a monoclonal anti-colony-stimulating factor 1 receptor antibody, in patients with advanced solid tumors. *Clin. Cancer Res.* **23**, 5703–5710 (2017).
 38. S. Bissinger, C. Hage, V. Wagner, I.-P. Maser, V. Brand, M. Schmittnaegel, A.-M. Jegg, M. Cannarile, C. Watson, I. Klamann, R. Rieder, A. Gonzalez Loyola, T. V. Petrova, P. A. Cassier, C. Gomez-Roca, V. Sibaud, M. De Palma, S. Hoves, C. H. Ries, Macrophage depletion induces edema through release of matrix-degrading proteases and proteoglycan deposition. *Sci. Transl. Med.* **13**, eabd4550 (2021).
 39. A. Lapenna, M. De Palma, C. E. Lewis, Perivascular macrophages in health and disease. *Nat. Rev. Immunol.* **18**, 689–702 (2018).
 40. H. He, J. J. Mack, E. Guc, C. M. Warren, M. L. Squadrito, W. W. Kilarski, C. Baer, R. D. Freshman, A. I. McDonald, S. Ziyad, M. A. Swartz, M. De Palma, M. L. Iruela-Arispe, Perivascular macrophages limit permeability. *Arterioscler. Thromb. Vasc. Biol.* **36**, 2203–2212 (2016).
 41. W. Swat, V. Montgrain, T. A. Doggett, J. Douangpanya, K. Puri, W. Vermi, T. G. Diacovo, Essential role of PI3K δ and PI3K γ in thymocyte survival. *Blood* **107**, 2415–2422 (2006).
 42. Y. Ben-Neriah, M. Karin, Inflammation meets cancer, with NF- κ B as the matchmaker. *Nat. Immunol.* **12**, 715–723 (2011).
 43. M. J. Smolinska, T. H. Page, A. M. Urbaniak, B. E. Mutch, N. J. Horwood, Hck tyrosine kinase regulates TLR4-induced TNF and IL-6 production via AP-1. *J. Immunol.* **187**, 6043–6051 (2011).
 44. X. Kong, Y. Liao, L. Zhou, Y. Zhang, J. Cheng, Z. Yuan, S. Wang, Hematopoietic cell kinase (HCK) is essential for NLRP3 inflammasome activation and lipopolysaccharide-induced inflammatory response *in vivo*. *Front. Pharmacol.* **11**, 581011 (2020).
 45. H. Yang, T. Yamazaki, F. Pietrocola, H. Zhou, L. Zitvogel, Y. Ma, G. Kroemer, STAT3 inhibition enhances the therapeutic efficacy of immunogenic chemotherapy by stimulating type 1 interferon production by cancer cells. *Cancer Res.* **75**, 3812–3822 (2015).
 46. M. Pascual-Garca, E. Bonfill-Teixidor, E. Planas-Rigol, C. Rubio-Perez, R. Iurlaro, A. Arias, I. Cuartas, A. Sala-Hojman, L. Escudero, F. Martinez-Ricarte, I. Huber-Ruano, P. Nuciforo, L. Pedrosa, C. Marques, I. Brana, E. Garralda, M. Vieito, M. Squatrito, E. Pineda, F. Graus, C. Espejo, J. Sahuquillo, J. Taberner, J. Seoane, LIF regulates CXCL9 in tumor-associated macrophages and prevents CD8(+) T cell tumor-infiltration impairing anti-PD1 therapy. *Nat. Commun.* **10**, 2416–2416 (2019).
 47. R. B. Delconte, T. B. Kolesnik, L. F. Dagley, J. Rautela, W. Shi, E. M. Putz, K. Stannard, J.-G. Zhang, C. Teh, M. Firth, T. Ushiki, C. E. Andoniou, M. A. Degli-Esposti, P. P. Sharp, C. E. Sanvitale, G. Infusini, N. P. D. Liao, E. M. Linossi, C. J. Burns, S. Carotta, D. H. D. Gray, C. Seillet, D. S. Hutchinson, G. T. Belz, A. I. Webb, W. S. Alexander, S. S. Li, A. N. Bullock, J. J. Babon, M. J. Smyth, S. E. Nicholson, N. D. Huntington, CIS is a potent checkpoint in NK cell-mediated tumor immunity. *Nat. Immunol.* **17**, 816–824 (2016).
 48. N. K. Brockwell, K. L. Owen, D. Zanker, A. Spurling, J. Rautela, H. M. Duivenvoorden, N. Baschuk, F. Caramia, S. Loi, P. K. Darcy, E. Lim, B. S. Parker, Neoadjuvant interferons: Critical for effective PD-1-based immunotherapy in TNBC. *Cancer Immunol. Res.* **5**, 871–884 (2017).
 49. L. C. Yao, K. E. Aryee, M. Cheng, P. Kaur, J. G. Keck, M. A. Brehm, Creation of PDX-bearing humanized mice to study immuno-oncology. *Methods Mol. Biol.* **1953**, 241–252 (2019).
 50. K. J. Livak, T. D. Schmittgen, Analysis of relative gene expression data using real-time quantitative PCR and the 2- $\Delta\Delta$ CT method. *Methods* **25**, 402–408 (2001).
 51. G. H. Nam, Y. Hong, Y. Choi, G. B. Kim, Y. K. Kim, Y. Yang, I. S. Kim, An optimized protocol to determine the engulfment of cancer cells by phagocytes using flow cytometry and fluorescence microscopy. *J. Immunol. Methods* **470**, 27–32 (2019).
 52. A. Butler, P. Hoffman, P. Smibert, E. Papalexis, R. Satija, Integrating single-cell transcriptomic data across different conditions, technologies, and species. *Nat. Biotechnol.* **36**, 411–420 (2018).
 53. D. Aran, A. P. Looney, L. Liu, E. Wu, V. Fong, A. Hsu, S. Chak, R. P. Naikawadi, P. J. Wolters, A. R. Abate, A. J. Butte, M. Bhattacharya, Reference-based analysis of lung single-cell sequencing reveals a transitional profibrotic macrophage. *Nat. Immunol.* **20**, 163–172 (2019).
 54. M. Goldman, B. Craft, M. Hastie, K. Repecka, F. McDade, A. Kamath, A. Banerjee, Y. Luo, D. Rogers, A. N. Brooks, J. Zhu, D. Haussler, The UCSC Xena platform for public and private cancer genomics data visualization and interpretation. bioRxiv 326470 (2019).
 55. A. M. Newman, C. L. Liu, M. R. Green, A. J. Gentles, W. Feng, Y. Xu, C. D. Hoang, M. Diehn, A. A. Alizadeh, Robust enumeration of cell subsets from tissue expression profiles. *Nat. Methods* **12**, 453–457 (2015).

Acknowledgments

Funding: This work was supported by National Health and Medical Research Council of Australia Project Grants 1025239, 1079257, 1081373, and 1092788 (M.E.); a National Health and Medical Research Council Investigator Grant (M.E.); a Cancer Council of Victoria Post-Doctoral Fellowship (A.R.P.); a Jack Brockhoff Foundation Early Career Research grant 4656-2019 (A.R.P.); a National Health and Medical Research Council of Australia Peter Doherty Early Career Fellowship GNT1166447 (A.R.P.); and an UC Cancer Research Coordinating Committee grant CRR-20-636450 (C.A.L.). **Author contributions:** Conception and design: A.R.P., W.S., F.J.P., and M.E. Development of methodology: A.R.P., W.S., F.J.P., and M.E. Acquisition of data: A.R.P., C.G.L., D.C., J.H.S., D.B., J.R., N.E., M.O., R.O., L.W., W.S., F.J.P., and M.E. Analysis and interpretation of data: A.R.P., C.G.L., D.C., J.H.S., D.B., M.C., S.N., J.R., N.D.H., N.E., M.O., R.O., L.G.E., C.M., J.D.M., L.W., G.G., L.B., A.L.C., C.A.L., W.S., F.J.P., and M.E. Writing, review, and/or revision of the manuscript: A.R.P., C.G.L., D.C., J.H.S., D.B., M.C., S.N., J.R., N.D.H., N.E., M.O., R.O., L.G.E., C.M., J.D.M., L.W., G.G., L.B., A.L.C., C.A.L., W.S., F.J.P., and M.E. Administrative, technical, or material support: A.R.P., C.G.L., D.C., J.H.S., D.B., M.C., S.N., J.R., N.D.H., N.E., M.O., R.O., L.G.E., C.M., J.D.M., L.W., G.G., L.B., A.L.C., C.A.L., W.S., F.J.P., and M.E. Study supervision: A.R.P., W.S., F.J.P., and M.E. Funding: A.R.P., F.J.P., and M.E. **Competing interests:** A.R.P. and M.E. are inventors on a

Therapeutic inhibition of the SRC-kinase HCK facilitates T cell tumor infiltration and improves response to immunotherapy

Ashleigh R. PohChristopher G. LoveDavid ChisangaJames H. SteerDavid BaloyanMichaël ChopinStephen NuttJai RautelaNicholas D. HuntingtonNima EtemadiMegan O'BrienRyan O'KeefeLesley G. ElliesChristophe MacriJustine D. MinternLachlan WhiteheadGangadhara GangadharaLouis BoonAshwini L. ChandClifford A. LowellWei ShiFiona J. PixleyMatthias Ernst

Sci. Adv., 8 (25), eabl7882. • DOI: 10.1126/sciadv.abl7882

View the article online

<https://www.science.org/doi/10.1126/sciadv.abl7882>

Permissions

<https://www.science.org/help/reprints-and-permissions>

Use of this article is subject to the [Terms of service](#)

Science Advances (ISSN) is published by the American Association for the Advancement of Science. 1200 New York Avenue NW, Washington, DC 20005. The title *Science Advances* is a registered trademark of AAAS.

Copyright © 2022 The Authors, some rights reserved; exclusive licensee American Association for the Advancement of Science. No claim to original U.S. Government Works. Distributed under a Creative Commons Attribution NonCommercial License 4.0 (CC BY-NC).